

Electronic supplementary information

Insights into the molecular composition of semi-volatile aerosols in the summertime central Arctic Ocean using FIGAERO-CIMS

Karolina Siegel^{a,b,c}, Linn Karlsson^{b,c}, Paul Zieger^{b,c}, Andrea Baccarini^{d,e}, Julia Schmale^{d,e}, Michael Lawler^f, Matthew Salter^{b,c}, Caroline Leck^{a,c}, Annica M. L. Ekman^{a,c}, Ilona Riipinen^{b,c}, and Claudia Mohr^{b,c,*}

^a Department of Environmental Science, Stockholm University, Stockholm, Sweden.

^b Department of Meteorology, Stockholm University, Stockholm, Sweden.

^c Bolin Centre for Climate Research, Stockholm University, Stockholm, Sweden.

^d Laboratory of Atmospheric Chemistry, Paul Scherrer Institute, Villigen PSI, Switzerland.

^e School of Architecture, Civil and Environmental Engineering, École Polytechnique Fédérale de Lausanne, Switzerland.

^f Department of Chemistry, University of California, Irvine, USA.

* Correspondence to: Claudia.Mohr@aces.su.se

Comparison of field blanks

Fig. S1 shows a mass spectra comparison between the field blanks **B1** and **B2**, a) for the first heatings (H1), b) the second heatings (H2, instrument background) and c) the instrument-background-subtracted signal (H1-H2). **B1** had an overall higher signal both in sample and background. In the analysis presented in this study, an average of the two blanks was used to correct for handling background in the samples.

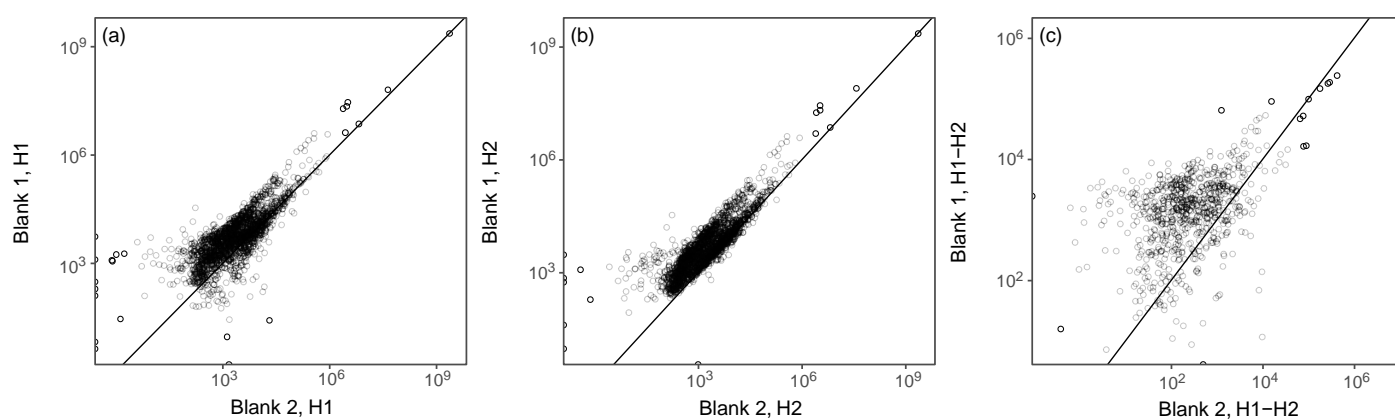


Figure S1 Integrated signal (mass per volume sampled [g m⁻³]) of mass spectra of Blank 1 (**B1**) and Blank 2 (**B2**), a) sample signal (heating 1, H1 in FIGAERO-CIMS), b) background signal (heating 2, H2), c) background-subtracted signal (H1-H2). The diagonal line represents a 1:1 relationship.

Instrument background correction for B1, F8 and F12

The second heating (instrument background) of the field blank sample **B1** and samples **F8** and **F12** exhibited a higher baseline compared to the first heating, which could also not be corrected for through the normalisation to the reagent ion. In order to still get meaningful (i.e. positive) data for these filters, we corrected the instrument backgrounds. For **B1** we used the ratio of the average signal of all data points below 40°C for the first and second heating (H1, H2) and adjusted the signal of H1 by this ratio, resulting in H1 corrected (Fig. S2). As we did not observe significant evaporation of sample compounds below 40°C, the signal in this temperature regime should be close to the instrument background.

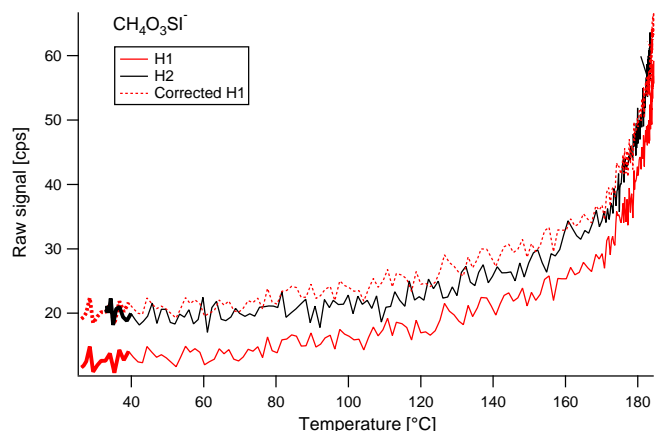


Figure S2 Thermogram of $\text{CH}_3\text{SO}_3\text{HI}^-$ (MSA) in Blank 1. The red solid line shows the sample signal (heating 1, H1) and the black solid line the background signal (heating 2, H2). The signal below 40°C is shown as a thicker line. After aligning the signals below 40°C, the resulting sample signal is shown as a dashed red line.

The backgrounds of **F8** and **F12** were approximated by the background signal of the average background signal (H2) of the two field blanks **B1** and **B2**, as the backgrounds for **F8** and **F12** were not correlated to the sample signal (see example thermogram in Fig. S3).

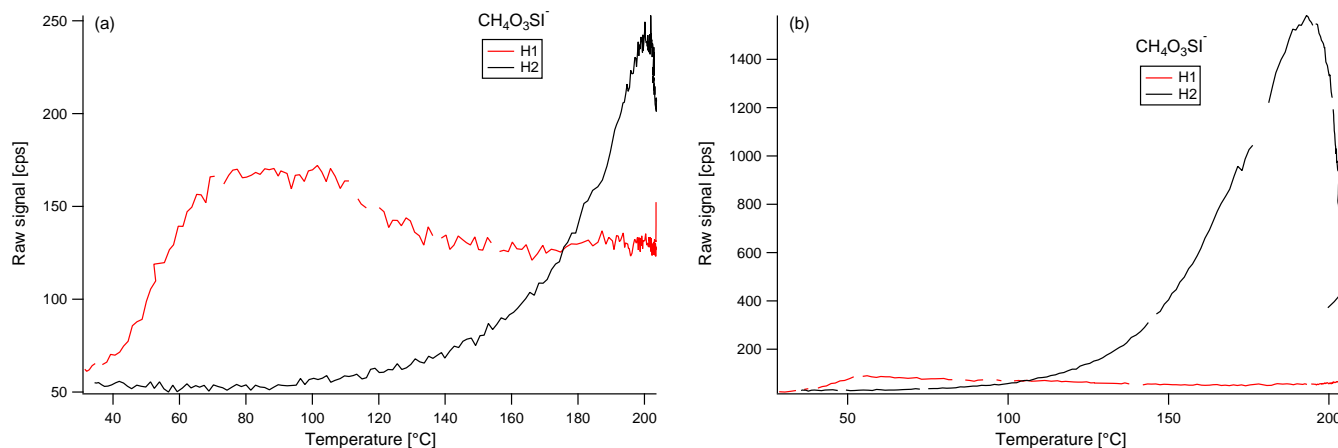


Figure S3 Time series of $\text{CH}_3\text{SO}_3\text{HI}^-$ (MSA) from a) Filter 8 (**F8**), and b) Filter 12 (**F12**) showing elevated background signal (heating 2, H2, black line) not correlated to the sample signal (heating 1, H1, red line).

Outliers and excluded compounds

Table S1 Field blank outliers that were excluded before the calculation of 1σ (standard deviation of the average field blank signal). The outliers were detected as signals exceeding the standard deviation (1σ) of the field blank average signal with the outliers included. The compounds are ordered from largest to smallest absolute value of their signal. Where a line (–) instead of a formula is given, no unambiguous molecular formula assignment could be achieved. Assigned ionic composition is given with the negative charge of -1 omitted. When iodide is not incorporated in the formula, the ionisation mechanism is uncertain.

Ionic formula	m/z	Ionic formula	m/z	Ionic formula	m/z
H ₂ IO	144.91504	CH ₂ IO ₂	172.90996	–	77.995308
C ₁₆ H ₃₂ IO ₂	383.14471	C ₁₅ H ₃₀ IO ₂	369.12906	–	94.025269
–	93.990227	C ₁₆ H ₃₀ IO ₂	381.12906	C ₁₈ H ₂₈ NO	274.2171
CO ₄	75.97966	C ₆ H ₁₅ INO ₇	339.98932	C ₁₆ H ₃₄ N ₃ O ₃	316.26001
C ₃ H ₆ IO ₃	216.93617	C ₁₈ H ₃₄ IO ₂	409.16034	C ₁₈ H ₂₄ NO ₈	382.15018
C ₁₈ H ₃₆ IO ₂	411.17599	–	92.010956	C ₁₆ H ₃₁ O ₂	255.23241
C ₃ H ₈ IO ₃	218.95181	CH ₄ IN ₂ O	186.93683	C ₁₀ H ₁₅ NO ₄ S	245.07217
CO ₃	59.984745	C ₁₃ H ₂₇ O ₁₄	407.14008	C ₂ H ₃ O ₂	59.013306
C ₁₄ H ₃₀ N ₃ O ₃	288.22873	C ₁₇ H ₂₆ NO	260.20145	C ₉ H ₆ NO	144.04494
C ₁₄ H ₂₈ IO ₂	355.1134	C ₁₇ H ₃₄ IO ₂	397.16034	C ₁₇ H ₃₆ NO ₃	302.26953

Table S2 Remaining signal (background-subtracted) of the aerosol filter samples after removal of signals below the LOD ($< 1\sigma$ of the background-subtracted field blank signal). All compounds above LOD (i.e. even non-iodide clusters) were included in the percentage. **F9** and to some extent **F5**, **F7** and **F13** seems to be lower due to a lower median signal in those filters, i.e. less sampled mass.

Sample	Signal remaining [%]
F1	97.16
F2	88.91
F3	99.16
F4	80.34
F5	79.39
F7	78.70
F8	95.12
F9	49.48
F10	84.09
F11	92.50
F12	92.94
F13	71.18

Contamination from ship pollution

The samples taken during the transit (**F8-F11**, Table 1 in the main article) **F8** and **F11** were classified as likely contaminated by pollution from the ship exhaust. The pollution influence can be shown when comparing the filter sampling times to integrated particle mass and black carbon mass concentrations, shown in Fig. S4. The elevated concentrations of sampled particle mass (especially for particles $< 1\mu\text{m}$) and black carbon (BC) on 2018-09-15–18 reflect the contamination by the ship engines during the transit. Data points from periods when the pumps for filter sampling were turned off have been removed to reflect the mass collected for FIGAERO-CIMS analysis.

Influence of inorganic sulfur, mainly sulfuric acid (H₂SO₄), can also be an indicator of ship contamination. Table S3 shows this clearly in **F11**. This information was however not used for distinguishing contamination in the samples. **F13** also had relatively higher signal from inorganic sulfuric compounds, despite that it was collected in the marginal ice zone under similar conditions as **F12**. The reason for this is most likely a lower overall remaining signal after background subtraction in **F13** (Table S2). As the signals of inorganic sulfuric compounds were commonly distinct, these signals were not as sensitive to background subtraction (i.e. were above LOD) as many of the organic compounds, and the relative contribution of inorganic sulfur compounds could therefore dominate. A similar effect appeared for **F7** and **F9**, which also had a low overall remaining signal and a notable contribution of inorganic sulfur. However, the remaining signal of **F5** was on a similar level as that of **F7**, and the shift towards relatively higher inorganic sulfur signal did not appear in **F5**.

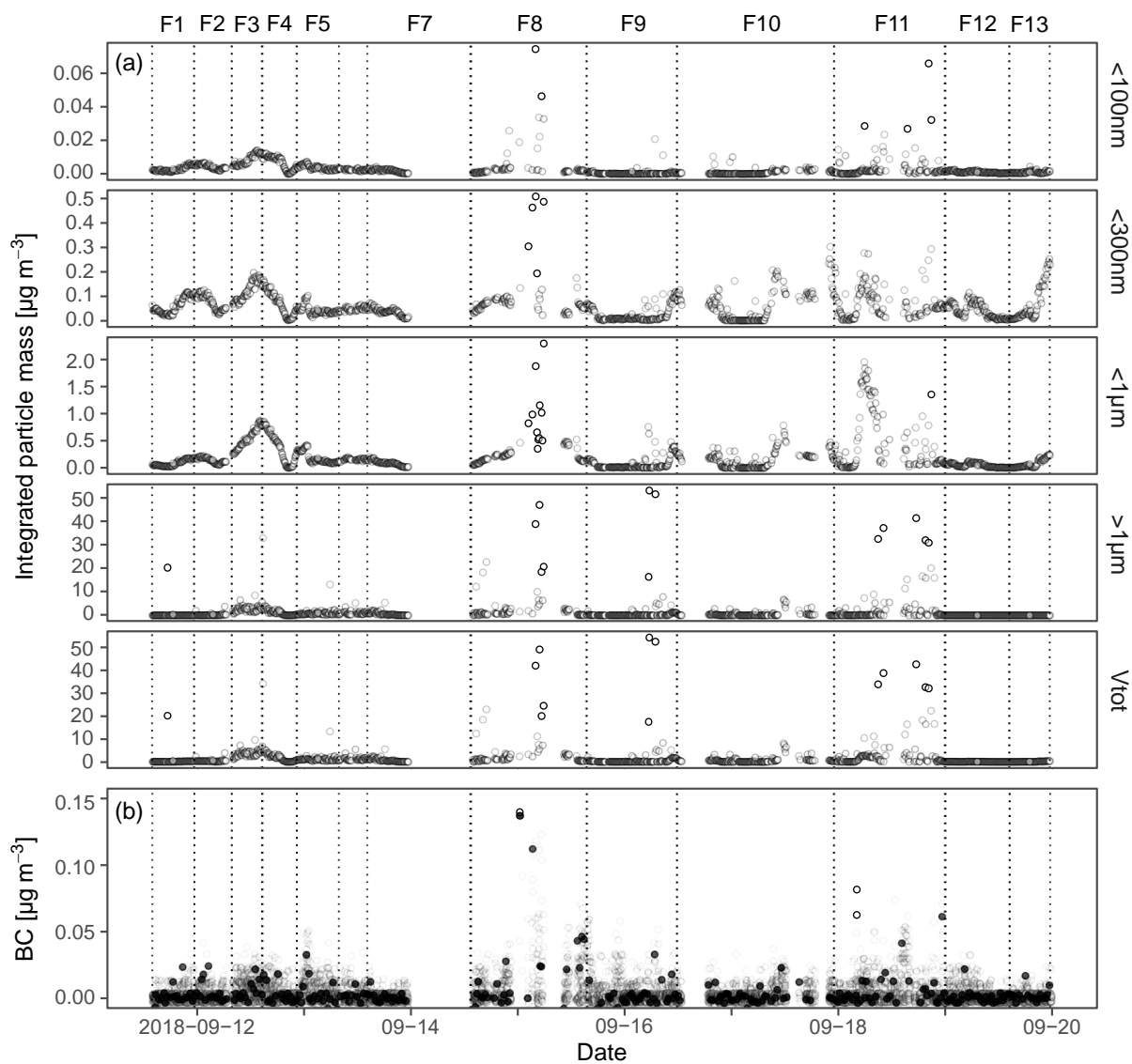


Figure S4 Time series of a) individual measurements of total integrated particle mass, separated by particle diameter (shown to the right of each panel), b) black carbon (BC). Circles represent individual measurements, and black dots (in b) 30 min averages. The integrated particle mass was derived from measurements of integrated particle volume and multiplied by an estimated density of 1.30 g cm^{-3} (see section 2.3 in the main article) for submicron particles and the density of sea salt (2.017 g cm^{-3}) for supermicron particles in this figure. Dashed vertical lines show start and end time of the aerosol samples **F1-F13**. The sample numbers are shown above the top panel.

Back trajectory averaging

Back trajectories (5 days) initiated from the 8 different levels (1-8, starting at 11-159 m altitude) within the boundary layer (BL) were averaged to one single trajectory. An example from 14 September, 00:00 UTC is shown in Fig. S5, where the coloured lines are the individual trajectories and the dashed black line is the averaged trajectory.

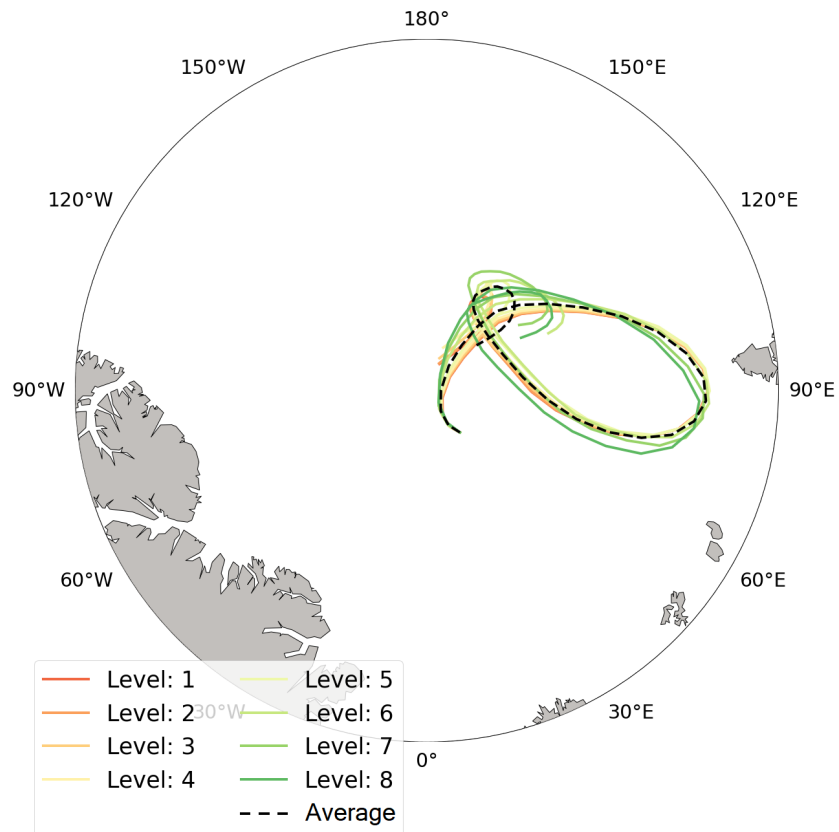


Figure S5 Example of 5-day back trajectories within the boundary layer from September 14, 00:00 UTC (coloured lines) used to calculate a single averaged trajectory (dashed black line). Level 1: starting at 11 m altitude; 2: 19 m; 3: 26 m; 4: 34 m; 5: 42 m; 6: 81 m; 7: 120 m; 8: 159 m.

Meteorological parameters

Meteorological parameters of importance for aerosol and cloud processes are shown in Fig. S6 for the measurement period 11-19 September 2018. Temperatures were consistently below zero and ranged from -15.1°C to -2.1°C during the sampling period. Relative humidity (RH) was at 100% on a few occasions and had a minimum value of 81.3%. Fog events (when the ground-level visibility was below 1000 m as defined by the World Meteorological Organization, WMO²), occurred frequently, especially in the period 16-18 September. Fog events often coincided with periods with a lower cloud base and a lower liquid water path. Downwelling shortwave radiation exhibited a diurnal cycle although the differences between day- and nighttime is very small at these latitudes during this time of the year. The wind speed (30 min average, Fig. 3c in the main article) ranged between 0.75 (17 September around 00:00 UTC) and 14.8 m s^{-1} (14 September around 23:30 UTC) with an average of 5.8 m s^{-1} .

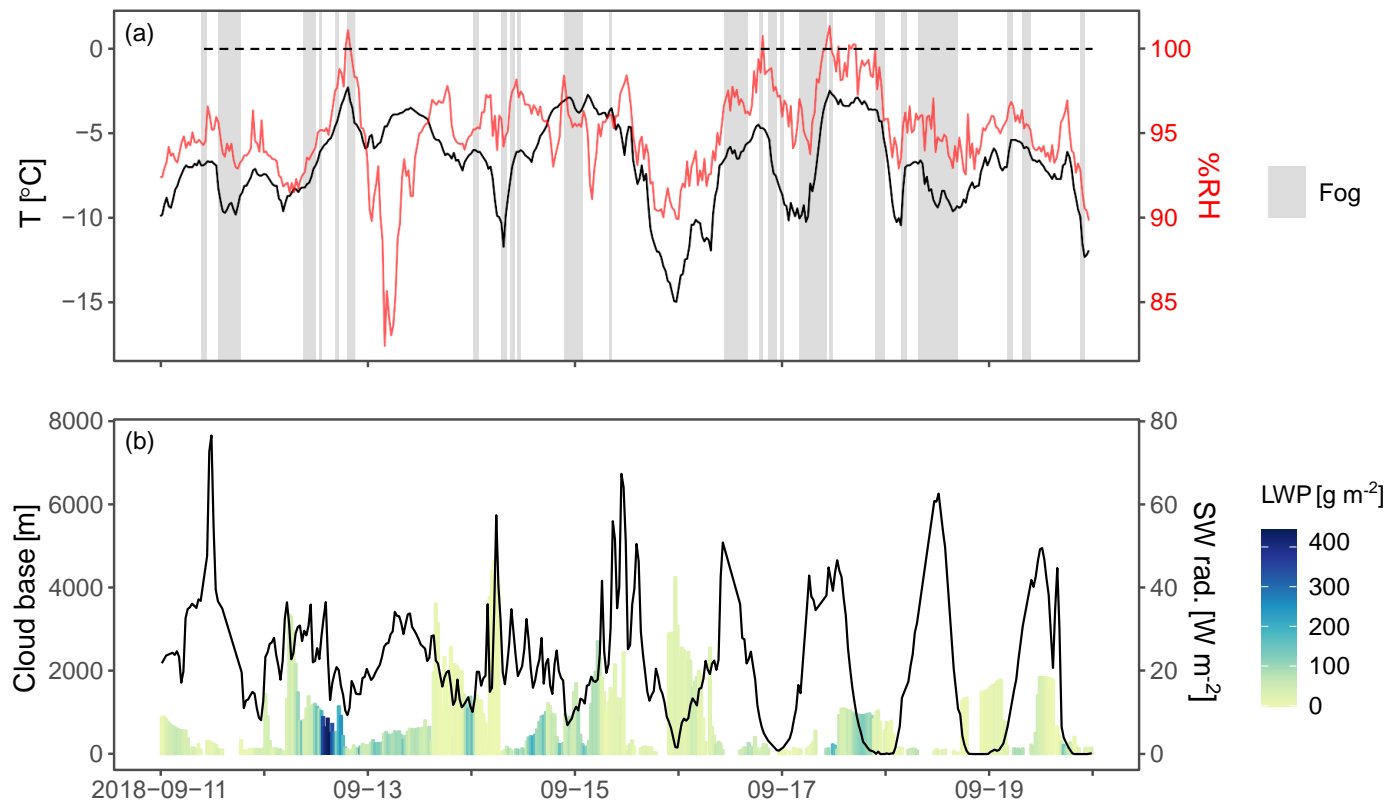


Figure S6 Meteorological parameters including a) temperature (T; black solid line), relative humidity (RH; red solid line) and fog as visibility < 1000 m (grey shaded areas), with the 0°C and 100% RH marked by a dashed line, b) liquid water path (LWP, colour bar), cloud base (bar height) and downwelling short-wave (SW) radiation (black line).

Aerosol chemical composition

Table S3 Relative contribution to the signal above background of the compound categories *CHO*, *CHON*, *CHONS*, *CHOS*, *Halogen* and *Inorg. S* in each of the aerosol filter samples **F1-F13**. The *Other* category was not included, as they were considered to be mainly contaminants from the instrument analysis and HNO_3^- in this category dominated the total signal intensity. The table corresponds to the pie charts shown in Fig. 2b in the main article.

Sample	<i>CHO</i> [%]	<i>CHON</i> [%]	<i>CHONS</i> [%]	<i>CHOS</i> [%]	<i>Halogen</i> [%]	<i>Inorg. S</i> [%]
F1	68	30	0	0	0	2
F2	74	17	0	4	0	5
F3	69	28	0	1	0	2
F4	84	10	0	0	2	4
F5	81	14	0	1	2	2
F7	80	11	0	0	2	7
F8	74	21	0	2	1	2
F9	90	1	0	0	1	8
F10	89	8	0	1	0	2
F11	21	9	0	7	0	63
F12	82	15	0	1	1	1
F13	65	12	0	6	0	17

Particle size distributions per filter sample periods

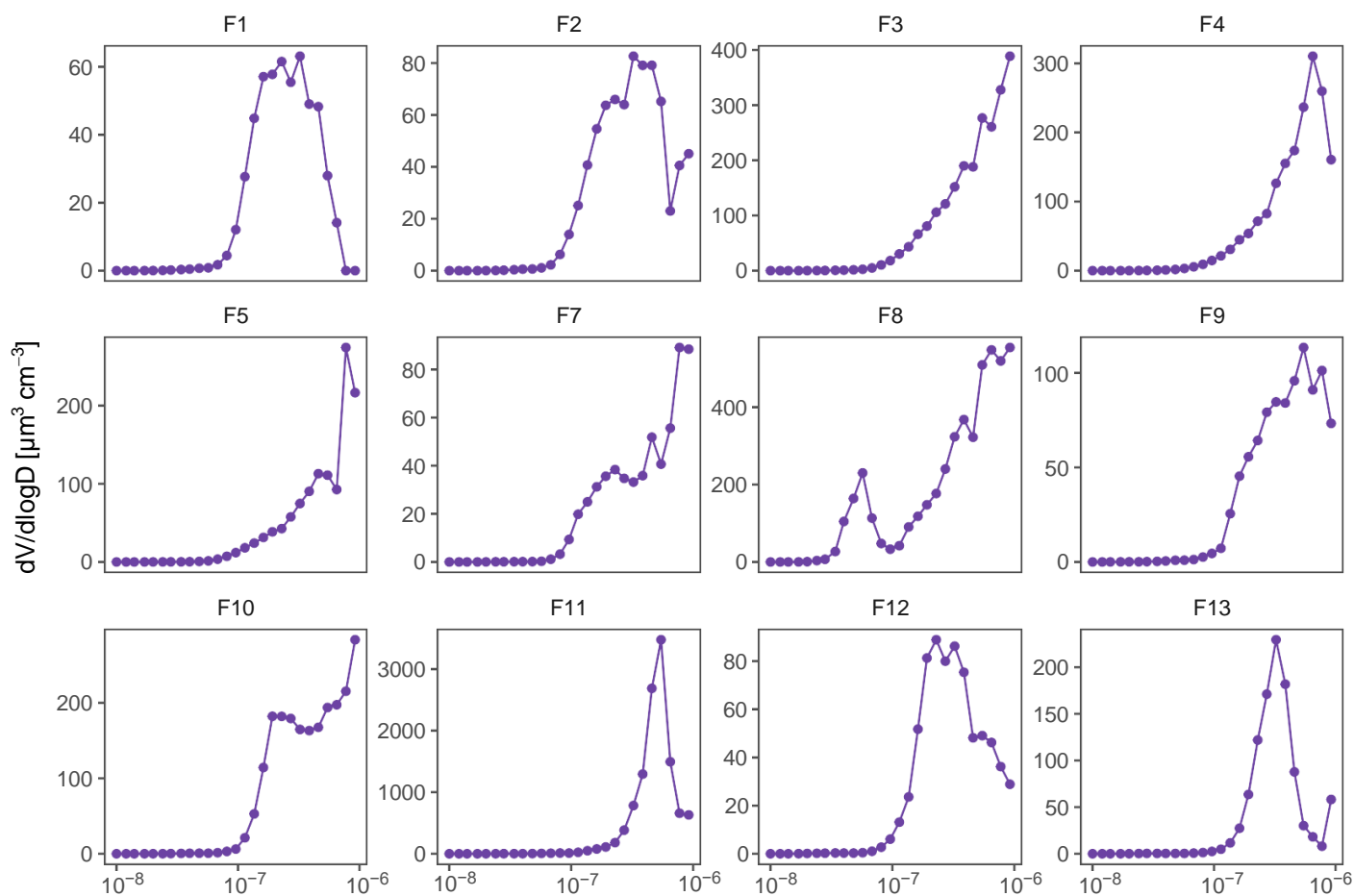


Figure S7 Summed volume size distributions for the collection periods of each aerosol sample **F1-F13**. D_p is the particle aerodynamic diameter.

Comparison of MSA, sulfuric acid and sulfate measurements of FIGAERO-CIMS to concurrent measurements

For the Particle-into-Liquid Sampler coupled to an Ion Chromatography Electrospray Ionization Tandem Mass Spectrometer (PILS-IC-ESI-MS/MS), submicron aerosol was collected through the PM₁ inlet into 1.5 mL vials using the PILS (Brechtel Manufacturing Inc., USA) with a typical sample time of 38 min. The samples were frozen and later analysed after the expedition with IC-ESI-MS/MS, using an ICS-2100 ion chromatograph and TSQ Quantum (Thermo Scientific, USA) as described in Grieman *et al.*³. The Thermal Desorption Chemical Ionization Mass Spectrometer (TDCIMS) measured the chemical composition of accumulation mode aerosol (~100-200 nm diameter) sampled through a PM₁₀ inlet occasionally in the field with 30-60 min collection periods as described in Lawler *et al.*⁴ and Smith *et al.*⁵. Only uncalibrated total counted ions are reported here for TDCIMS.

The comparison of these three techniques for MSA and sulfuric acid, and sulfate (SO₄²⁻) and CH₃SO₂ (a proxy for MSA) measured by AMS is presented in Fig. S8. The figure shows that, although using different time periods for integration, there is conformation especially for the sulfate measurements during the more controlled conditions of the ice drift (F1-F7). A major outlier of FIGAERO-CIMS is the high MSA signal in F13, which is not supported by the AMS, PILS-IC-ESI-MS/MS and TDCIMS. The FIGAERO-CIMS mass spectrum showed no signs of over-fitting or presence of multiple peaks in F13, and the reason for this high signal is therefore not clear.

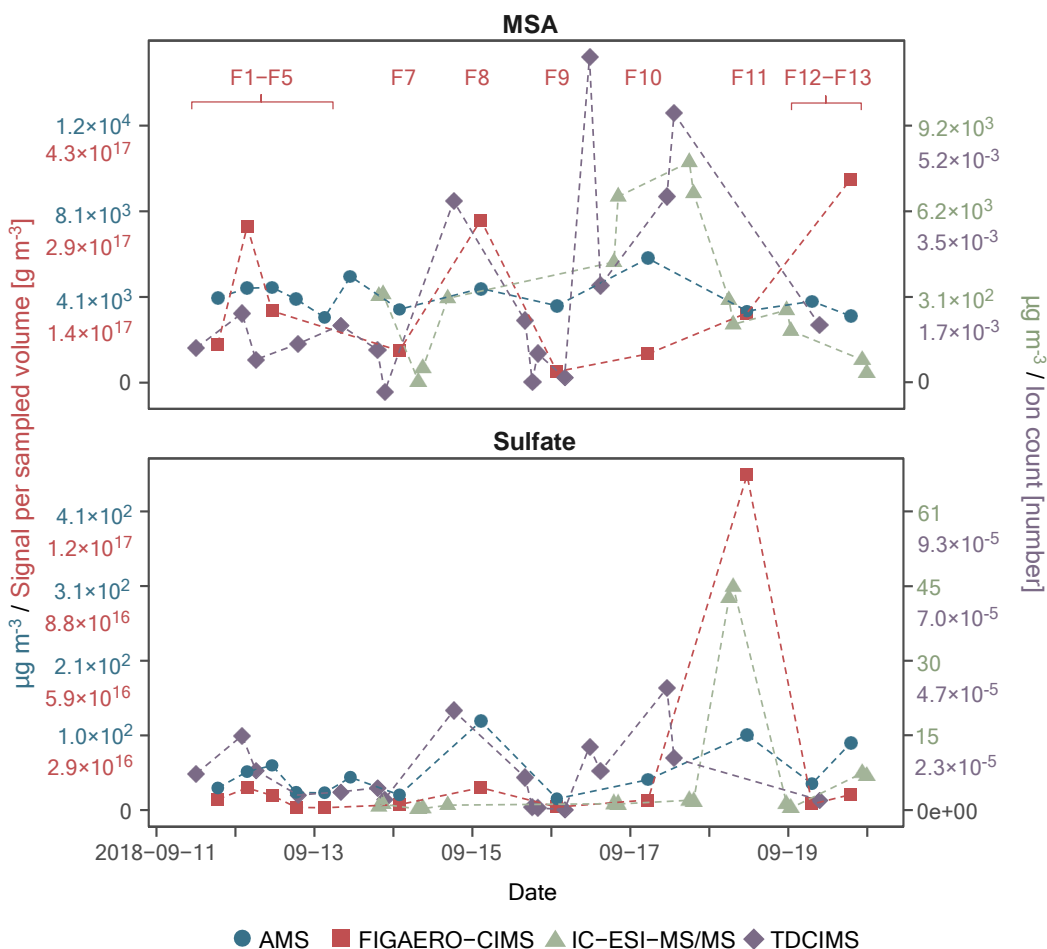


Figure S8 Time series of MSA (p) (upper) and sulfuric acid/sulfate (p) (lower) measured by AMS (PM₁), FIGAERO-CIMS (whole-air), IC-ESI-MS/MS (PM₁) and TDCIMS (PM₁₀).

Carbon number and oxygen-to-carbon ratio

Table S4 Number of carbons (C1-C20) and oxygen to carbon (O : C) ratio in the aerosol samples (filter median signals > LOD). The C categories represent the number of carbons in the compound and the values in the CHO, CHON, CHONS and CHOS columns represent the number of compounds within that compound and C category.

C category	CHO	CHON	CHONS	CHOS
C1	5	0	2	2
C2	5	4	0	3
C3	9	8	0	4
C4	14	13	0	1
C5	24	16	1	1
C6	27	15	0	1
C7	31	22	0	0
C8	30	22	0	3
C9	20	17	1	0
C10	27	20	0	0
C11	17	11	0	0
C12	16	17	0	0
C13	17	7	0	0
C14	10	5	0	0
C15	14	7	0	0
C16	11	2	0	0
C17	3	2	0	0
C18	5	2	0	0
C19	0	0	0	0
C20	0	0	0	0
Σ C1-C20	285	190	4	15
Average C number	8.96	8.58	4.00	3.93
O : C ratio	0.692	0.627	1.33	1.34

DMS measurements

Measured DMS concentrations during the measurement period ranged between 0.055 and 2.0 nmol m⁻³, with a median of 0.68 nmol m⁻³. The highest concentration (2.0 nmol m⁻³) was measured on 17 September at 04:22 and the lowest concentration (0.055 nmol m⁻³) on 14 September at 15:55. A comparison to measured atmospheric DMS concentrations during previous expeditions with I/B *Oden* are shown in Table S5. Our measured concentrations during the ice drift, 0.85 nmol m⁻³ (median) were at a similar level (or slightly lower) compared to IAOE-91, AOE-2001 and ASCOS, but ~ 3 times lower than during AOE-96. However, it is inappropriate to draw conclusions simply based upon these numbers since both the location and time of year varied within the range of mid July - mid September. Leck and Persson^{6,7} concluded that DMS in seawater and air samples decreased by 20-30% per week in the central Arctic Ocean during the summer to autumn freeze-up. Therefore, the numbers we report here are only for a rough comparison and to demonstrate environmental variability between the data sets.

Table S5 Median measured ambient DMS and 5th and 95th percentiles during the five expeditions to the central Arctic Ocean north of 80° N with I/B *Oden*. For easier comparison of MOCCHA to previous expeditions, median concentrations during MOCCHA are given both for the entire ice drift and for the dates for aerosol sampling in this study. The DMS measurements during MOCCHA started two days later than the beginning of the ice drift due to technical issues.

Campaign	Date (DoY)	Median ambient DMS (nmol m ⁻³)	Percentiles (5 th , 95 th)
IAOE-91 ^a	1 August–6 October 1991 (213-279)	0.91	0.23, 3.85
AOE-96 ^a	18 July–23 August 1996 (200-236)	2.68	0.68, 11.8
AOE-2001 ^a	15–26 August 2001 (227-238)	1.07	0.27, 4.44
ASCOS ^b	12 August–2 September 2008 (225-246)	0.76	0.34, 3.57
MOCCHA (ice drift)	15 August–14 September 2018 (227-257)	0.85	0.15, 2.60
MOCCHA (this study)	11–19 September 2018 (254-262)	0.68	0.11, 1.76

^a Leck and Persson⁷, Lundén *et al.*⁸

^b Leck, *personal comm.*, 2020-07-14

Notes and references

- [1] P. Zieger, O. Väisänen, J. C. Corbin, D. G. Partridge, S. Bastelberger, M. Mousavi-Fard, B. Rosati, M. Gysel, U. K. Krieger, C. Leck, A. Nenes, I. Riipinen, A. Virtanen and M. E. Salter, *Nature communications*, 2017, **8**, 1–10.
- [2] P. J. Croft and B. Ward, *CLOUDS AND FOG | Fog*, Academic Press, Oxford, 2015, pp. 180–188.
- [3] M. M. Grieman, M. Aydin, D. Fritzsche, J. R. McConnell, T. Opel, M. Sigl and E. S. Saltzman, *Climate of the Past*, 2017, **13**, 395–410.
- [4] M. J. Lawler, M. P. Rissanen, M. Ehn, R. L. Mauldin III, N. Sarnela, M. Sipilä and J. N. Smith, *Geophysical Research Letters*, 2018, **45**, 2038–2046.
- [5] J. Smith, K. Moore, P. H. McMurry and F. Eisele, *Aerosol Science and Technology*, 2004, **38**, 100–110.
- [6] C. Leck and C. Persson, *Tellus B: Chemical and Physical Meteorology*, 1996, **48**, 156–177.
- [7] C. Leck and C. Persson, *Tellus B: Chemical and Physical Meteorology*, 1996, **48**, 272–299.
- [8] J. Lundén, G. Svensson and C. Leck, *Journal of Geophysical Research: Atmospheres*, 2007, **112**, D11308.